# Identification of metabolites associated with capecitabine-induced hand-foot syndrome using untargeted metabolomics in patients with cancer

YURU BAI[1*], HONG CHEN[1*], LEYING GU[2], BO SHI[3], ZHEN WANG[1], YUANYUAN DUANMU[1], YING HU[1], YU WANG[1], CHAOYI ZHANG[1] and ZHAOTIAN SU[1]

[1]Department of Oncology, Nanjing Jiangning Hospital of Traditional Chinese Medicine Affiliated to China Pharmaceutical University, Nanjing, Jiangsu 211100, P.R. China; [2]Department of Basic Medicine, College of Health and Nursing, Wuxi Taihu University, Wuxi, Jiangsu 214063, P.R. China; [3]Department of Laboratory Medicine, Nanjing Jiangning Hospital of Traditional Chinese Medicine Affiliated to China Pharmaceutical University, Nanjing, Jiangsu 211100, P.R. China

Received December 6, 2024; Accepted April 1, 2025

DOI: 10.3892/mmr.2025.13568

**Abstract.** Hand-foot syndrome (HFS) is defined as a major adverse reaction to capecitabine; however, the underlying mechanisms remain unclear. In total, 85 patients who were taking oral capecitabine were included in the present study and these patients were divided into HFS-positive and HFS-negative groups. Serum samples were collected from patients and an untargeted metabolomics analysis was conducted using ultra-high performance liquid chromatography-mass spectrometry/mass spectrometry. The present study aimed to investigate the presence of metabolites in the serum of patients that developed HFS in response to capecitabine treatment. A total of 193 differential metabolites were identified, with 134 upregulated and 59 downregulated. Bioinformatics analysis revealed four novel metabolites that may be associated with HFS. Subsequent *in vitro* experiments were conducted to explore the damaging effects of capecitabine and its associated metabolites on human adult keratinocyte cell line, TPA-treated (HaCaT) cells. Results of the present study revealed that aciclovir and lamivudine affected cellular damage at the highest level. In conclusion, the present study aimed to systematically and comprehensively describe the metabolites present in patients with capecitabine-induced HFS and may further the current understanding of the capecitabine pathways that play a key role in HFS.

*Correspondence to:* Dr Yuru Bai, Department of Oncology, Nanjing Jiangning Hospital of Traditional Chinese Medicine Affiliated to China Pharmaceutical University, 657 Tianyin Avenue, Nanjing, Jiangsu 211100, P.R. China
E-mail: yuru6197@gmail.com

Professor Leying Gu, Department of Basic Medicine, College of Health and Nursing, Wuxi Taihu University, 68 Qianrong Road, Wuxi, Jiangsu 214063, P.R. China
E-mail: 13852292155@163.com

*Contributed equally

*Key words:* hand-foot syndrome, capecitabine, ultra-high performance liquid chromatography-mass spectrometry, mass spectrometry differential metabolites

## Introduction

Capecitabine (CAP), an inactive pro-drug form of 5-fluorouracil (5-FU), is widely used in the treatment of solid tumors, including colorectal, breast, gastric, pancreatic and biliary tract cancer (1,2). Following oral intake, CAP is absorbed through the gastrointestinal tract, where it undergoes three enzymatic conversions to become active 5-FU. Initially, CAP is converted to 5'-dFCR by carboxlesterase, which is transformed into 5'-dFUR by cytidine deaminase. Subsequently, 5-FU is produced by thymidine phosphorylase and the active form of 5-FU and its metabolites exert therapeutic effects within tumor cells (3-5).

Hand-foot syndrome (HFS), also known as palmar-plantar erythrodysesthesia, is the most commonly reported side effect of oral capecitabine therapy, occurring in >50% of patients (6). HFS is characterized by distinct erythema and palmoplantar dysesthesia and patients with this disease may experience edema, skin peeling and fissures on the fingers or toes, which can progress to blistering, ulceration and full-thickness skin necrosis (7). Severe pain associated with HFS often impairs a patient's ability to perform daily activities. Thus, reductions in dosage or drug discontinuation may be required, compromising the efficacy of this chemotherapy (8). Although various mechanisms for capecitabine-induced HFS have previously been suggested, including cox inflammatory reactions, metabolic enzymes, transporters involved in drug absorption and genetic variations, the specific mechanisms remain to be fully elucidated (9). Research continues; however, effective prevention and treatment options are lacking due to the incomplete understanding of the specific causes of HFS (10,11).

The present study aimed to examine the differential metabolites between capecitabine-treated patients with and

without HFS. Untargeted metabolomics was performed using ultra-high performance liquid chromatography-mass spectrometry/mass spectrometry (UHPLC-MS/MS) to determine novel metabolites of capecitabine that may be associated with HFS development.

In addition, specific metabolites associated with capecitabine were verified at the cellular level, enhancing the current understanding of the metabolic activation involved in capecitabine-induced HFS. Collectively, results of the present study may provide a theoretical basis for novel therapeutic strategies to be used in the treatment of HFS.

## Materials and methods

*Patients*. Between March 2021 and March 2023, a total of 85 patients who received capecitabine chemotherapy were admitted to the Oncology Department of Nanjing Jiangning Hospital of Traditional Chinese Medicine. The present study was approved by the Institutional Ethics Committee of Nanjing Jiangning Hospital of Traditional Chinese Medicine (approval no. JZL-2021-08K-01) and all patients provided written informed consent. Patients were included in the present study according to the following criteria: i) The presence of malignant tumors confirmed through pathology, histology or cytology; ii) the presence of any malignant tumors treated with capecitabine chemotherapy, including adjuvant/neoadjuvant therapy or palliative care; iii) aged 18-85 years; iv) Karnofsky Performance Status (KPS) (12) score of ≥60; v) expected survival time of >3 months; and vi) concurrent radiotherapy or biological treatments, such as trastuzumab or bevacizumab (that do not cause HFS or neuropathy). Patients were excluded from the present study according to the following criteria: i) Not meeting the inclusion criteria; ii) poor treatment compliance and an inability to cooperate with treatment; iii) a loss to follow-up during the medication intervention period; and iv) voluntary withdrawal from treatment. Exit criteria was as follows: i) The presence of severe adverse reactions, including skin allergic reactions or rashes, leading to trial discontinuation; and ii) worsening of conditions, leading to death. The primary characteristics of patients are summarized in Table I.

*Sample collection and preparation*. All patients received oral capecitabine (cat. no. 1D0733DE3; Qilu Pharmaceutical Co., Ltd.) for chemotherapy. Capecitabine was administered orally twice daily (morning and evening) at a dosage of 1,250 mg/m$^2$. The treatment regimen included two weeks of medication followed by a one-week break, with each treatment cycle lasting three weeks. Patients completed at least three consecutive cycles. According to the National Cancer Institute's Common Terminology Criteria for Adverse Events (CTCAE; version 5.0) (13), grade 0 was classified as HFS-negative, while grades 1-3 were classified as HFS-positive. Patients were divided into two groups according to HFS status, with 42 patients who were HFS-negative and 43 patients who were HFS-positive. Following the completion of five treatment cycles, patients fasted for at least 6 h prior to blood sample collection. Blood samples were centrifuged at 4˚C, 2,352 x g for 5 min to obtain plasma and this was stored at -80˚C.

Samples were obtained from each group for lipid extraction and these were randomly combined to form 23 pooled samples. In total, 100 $\mu$l of each liquid sample was extracted using 400 $\mu$l of methanol:acetonitrile (ratio, 1:1). The mixture was sonicated at 40 kHz for 30 min at 5˚C and samples were subsequently stored at -20˚C for 30 min to precipitate the proteins. Following centrifugation at 13,000 x g and 4˚C for 15 min, the supernatant was transferred to new microtubes and evaporated to dryness under nitrogen.

For UHPLC-MS/MS analysis, samples were reconstituted in 100 $\mu$l of acetonitrile:water (ratio, 1:1) solution using sonication in a 5˚C water bath. The reconstituted metabolites were centrifuged at 13,000 x g and 4˚C for 15 min and the supernatant was transferred to sample vials for LC-MS/MS analysis. As part of system conditioning and quality control (QC), a pooled QC sample was prepared by mixing equal volumes of all samples. QC samples were processed and tested in the same manner as the analytic samples. The complete sample set was injected at regular intervals to monitor the stability of the analysis.

*UHPLC-MS/MS analysis*. UHPLC-MS/MS analysis was performed using the UHPLC-Q Exactive HF-X system (Thermo Fisher Scientific, Inc.).

*Chromatographic conditions*. A 2-$\mu$l sample was separated prior to MS using an HSS T3 column (100x2.1 mm i.d.; 1.8 $\mu$m). Mobile phases consisted of solvent A (0.1% formic acid in water:acetonitrile; ratio, 95:5) and solvent B (0.1% formic acid in acetonitrile:isopropanol:water; ratio, 47.5:47.5:5). The solvent gradient was as follows: From 0-3.5 min, 0% B-24.5% B (0.4 ml/min); from 3.5-5 min, 24.5% B-65% B (0.4 ml/min); from 5-5.5 min, 65% B-100% B (0.4 ml/min); from 5.5-7.4 min, 100% B maintained with a flow rate increasing from 0.4-0.6 ml/min; from 7.4-7.6 min, 100% B-51.5% B (0.6 ml/min); from 7.6-7.8 min, 51.5% B-0% B (0.6-0.5 ml/min); from 7.8-9 min, 0% B (0.5-0.4 ml/min); and from 9-10 min, 0% B (0.4 ml/min) for system equilibration. The sample injection volume was 2 $\mu$l with a flow rate set-0.4 ml/min and the column temperature was maintained at 40˚C. All samples were stored at 4˚C during the analysis.

*MS conditions*. The mass spectrometric data was collected using a Thermo UHPLC-Q Exactive HF-X Mass Spectrometer (Thermo Fisher Scientific, Inc.) equipped with an electrospray ionization source, operating in both positive and negative ion modes. The optimal conditions were set as follows: Heater temperature, 425˚C; capillary temperature, 325˚C; sheath gas flow rate, 50 arb; auxiliary gas flow rate, 13 arb; ion-spray voltage floating, at -3,500 V in negative mode and 3,500 V in positive mode; and normalized collision energy set at 20-40-60 V for MS/MS. The full MS resolution was 60,000 and MS/MS resolution was 7,500. Data acquisition was performed in Data Dependent Acquisition (DDA) mode, covering a mass range of 70-1,050 m/z.

*Data pre-processing and annotation*. Following detection using MS, the raw data obtained using LC/MS were pre-processed using Progenesis software (QI; Waters Corporation). This process exported a three-dimensional data matrix in CSV format, containing sample information, metabolite names and mass spectral response intensities.

Table I. Clinical characteristics of patients.

| Item | HFS negative | HFS positive | P-value |
|---|---|---|---|
| Sex | | | 0.76[a] |
| Male | 25 | 27 | |
| Female | 17 | 16 | |
| Age, years | 25-85 | 38-80 | 0.09[b] |
| Mean age | 64.31±14.23 | 59.35±12.14 | |
| Tumor type | | | 0.65[a] |
| Gastric cancer | 17 | 20 | |
| Colorectal cancer | 16 | 17 | |
| Others | 9 | 6 | |

[a]$\chi^2$ test; [b]Student's unpaired t-test. HFS, hand-foot syndrom.

Internal standard peaks, along with known false positives, such as noise, column bleed and derivatized reagent peaks, were removed from the matrix. Data were de-duplicated and peak-pooled. Metabolites were identified using Human Metabolome Database (HMDB) (version 4.0; http://www.hmdb.ca), Metlin (https://metlin.scripps.edu; version 2021) and Majorbio Database (https://www.majorbio.com; version 2022).

Processed data were uploaded to the Majorbio cloud platform (https://cloud.majorbio.com) for further analysis. Metabolic features detected in ≥80% of any sample set were retained. Post-filtering, minimum values were entered for metabolites that fell below the quantitation limit in specific samples. Each metabolic feature was normalized using the sum normalization method to minimize errors from sample preparation and instrument instability, resulting in a normalized data matrix. Variables with a relative standard deviation of >30% in QC samples were excluded and the data were $\log_{10}$-transformed to produce the final data matrix for subsequent analysis.

*Differential metabolites data analysis*. Following pre-processing of the data matrix, Principal component analysis (PCA) and orthogonal least partial squares discriminant analysis (OPLS-DA) were performed using the R package, ropls (version, 1.6.2; https://cran.r-project.org/web/packages/ropls/) (14). Overall data analysis was conducted using R (R Core Team, http://www.R-project.org/). A 7-fold cross-validation (>1.5 for upregulated and <0.67 for downregulated) and statistical significance (P<0.05) was used to assess model stability and robustness. Additionally, permutation tests were conducted to validate the models, ensuring that the observed group separation was statistically significant and not due to random chance. To identify markedly differential metabolites, the present study employed a combination of univariate and multivariate statistical methods. Student's unpaired t-tests and fold difference analysis were conducted to evaluate individual metabolite changes between groups. Markedly differential metabolites were identified based on the variable importance in the projection (VIP) from the OPLS-DA model and the P-value from Student's t-test. Metabolites with VIP >1 and P<0.05 were considered statistically significant (15), resulting in the identification of 193 differential metabolites.

The aforementioned metabolites were categorized and mapped to their biochemical pathways using metabolic enrichment and pathway analysis, through the Kyoto Encyclopedia of Genes and Genomes (KEGG) database (http://www.genome.jp/kegg/). Metabolites were classified according to the associated pathways or functions. Enrichment analysis was performed to determine whether specific functional groups of metabolites were present. This process extended the annotation from single metabolites to groups of metabolites. The Python package scipy.stats (https://docs.scipy.org/doc/scipy/) was used to identify statistically significant enriched pathways using Fisher's exact test. These metabolites are strongly associated with neurotoxicity, immunomodulatory effects and inflammatory responses. They exhibited the highest fold changes and statistical significance between the HFS-positive and HFS-negative groups. Notably, these metabolites have not been previously reported in the context of capecitabine-induced toxicity, highlighting their potential as novel biomarkers or therapeutic targets for managing capecitabine-related adverse effects.

*Cell culture and treatment*. HaCaT immortalized epidermal cells (cat. no. iCell-h066; iCell) were cultured in Dulbecco's Modified Eagle's Medium (DMEM) (cat. no. 11965-092; Thermo Fisher Scientific, Inc.) supplemented with 10% fetal bovine serum (FBS) (cat. no. 26140-079; Thermo Fisher Scientific, Inc.) and 1% penicillin-streptomycin (cat. no. 15140-122; Thermo Fisher Scientific, Inc.). The culture environment was maintained at 37˚C with 5% $CO_2$. When the cells reached 80-90% confluence, cells were treated with a 0.25% trypsin-0.02% EDTA solution (w/v) for 5 min at 37˚C. Subsequently, cells were resuspended in DMEM with 10% FBS to reach a final concentration of $2x10^5$ cells/ml and plated onto 96-well plates for cell damage assays.

HaCaT cells had been used previously in other institutions and authentication was conducted using short tandem repeat (STR) profiling following the storage of cell seeds. Cell detection was performed following DNA extraction using Axygen's genome extraction kit (Axygen Scientific, Inc.). The 21-STR amplification protocol was used to amplify and detect the STR locus and sex gene amelogenin on the ABI 3730XL genetic analyzer (Applied Biosystems; Thermo Fisher Scientific, Inc.). STR profiles were compared using the Deutsche Sammlung von Mikroorganismen und Zellkulturen (DSMZ) online STR analysis tool (https://celldive.dsmz.de/str,accessed). This tool encompasses STR data from 2,455 cell lines sourced from major repositories, including the American Type Culture Collection, DSMZ, Japanese Collection of Research Bioresources and Rikagaku Kenkyūjo databases.

*Cell Counting Kit-8 (CCK-8) assay*. Cell damage was assessed using a CCK-8 assay. HaCaT cells were divided into blank control, capecitabine and metabolite groups. Metabolites included aciclovir (cat. no. HY-17422; MedChemExpress), genistein (cat. no. HY-14596; MedChemExpress), Lamivudine (cat. no. HY-B0250; MedChemExpress) and Lomerizine (cat. no. HY-B0768A; MedChemExpress). Cells were inoculated in 96-well plates and treated with various concentrations

of capecitabine and its metabolites (0.001, 0.01, 0.1, 1, 10, 100, 200 and 400 $\mu$M). Following incubation for 48 h at 37˚C, 10 $\mu$l of CCK-8 solution (cat. nos. HYCEZMBIO and HYCCK8-500T) were added to each well and gently mixed. Plates were subsequently incubated for an additional 1-4 h in an incubator (model, 3311; Thermo Fisher Scientific, Inc.). Absorbance was measured at a wavelength of at 450 nm using a microplate reader (model AMR-100; Hangzhou Aoshen Instrument Co., Ltd.) and the average optical density for each well was calculated. Cytotoxicity was analyzed through comparison with the blank control group. A dose-response curve was plotted, the half-maximal inhibitory concentration ($IC_{50}$) was calculated and aciclovir and lamivudine were identified as causing the highest levels of cell damage.

*Hoechst 33258 staining*. HaCaT cells were divided into the following groups: i) Blank control group; ii) 50% $IC_{50}$ capecitabine group; iii) $IC_{50}$ capecitabine group and iv) metabolite group (including acyclovir and lamivudine). Following treatment for 48 h at 37˚C, culture medium was removed and 0.5 ml of fixative solution (4% paraformaldehyde; cat. no. 80096618; Sinopharm Chemical Reagent Co., Ltd.) was added to fix the cells on coverslips for 15 min. Cells were subsequently washed three times with PBS, with each wash lasting 3 min and the residual PBS was removed using absorbent paper. Subsequently, 0.5 ml of Hoechst 33258 staining solution (5 mg/l; cat. no. C1018; Beyotime Institute of Biotechnology) was added and cells were incubated at room temperature for 5 min. Cells were washed a further three times with PBS, with each wash lasting 3 min. A drop of anti-fade mounting medium (cat. no. 0100-1; SouthernBiotech) was added and the coverslips were mounted. Cell morphology was observed under a fluorescence microscope (ECLIPSE Ci; Nikon Corporation).

*Annexin V/PI staining*. HaCaT cells were divided into the following groups: i) Blank control group; ii) 50% $IC_{50}$ capecitabine group; iii) $IC_{50}$ capecitabine group and iv) metabolite group (including acyclovir and lamivudine). The cells were digested with 0.25% trypsin without EDTA at 37˚C for 2-3 min. After stopping the digestion, the treated cells were collected and centrifuged at 215 x g for 5 min at 4˚C. The supernatant was discarded and the pellet resuspended in PBS. the cells were washed twice with PBS by centrifugation at 215 x g for 5 min at 4˚C each time. The Annexin V-APC/7-AAD apoptosis detection kit (KGA1106-100; KeyGEN BioTECH) was used for analysis. 7-AAD staining solution (5 $\mu$l) was added to 50 $\mu$l of Binding Buffer and mixed well. The prepared 7-AAD staining solution was added to the collected cells and mixed well before incubation at room temperature in the dark for 5-15 min. Following incubation, 450 $\mu$l of Binding Buffer was added and mixed well. Annexin V-APC (5 $\mu$l) was added and mixed well before incubation at room temperature in the dark for 5-15 min. Flow cytometry was performed using the CytoFLEX flow cytometer (Beckman Coulter) equipped with CytExpert software (version 2.4; Beckman Coulter). Data analysis was conducted using FlowJo software (FlowJo, LLC). After staining and labeling the cells, multicolor compensation was set up in the CytExpert software prior to data acquisition.In FlowJo, cell debris and aggregates were excluded by gating based on forward scatter (FSC) and side scatter (SSC). A dot plot of Annexin V (X-axis) vs. PI (Y-axis) was used to identify four quadrants: LL (Annexin V-/PI-): Viable cells,LR (Annexin V+/PI-): Early apoptotic cells,UR (Annexin V+/PI+): Late apoptotic cells,UL (Annexin V-/PI+): Necrotic cells.The total apoptosis rate was calculated using the following formula:Total apoptosis rate (%)=(Number of early apoptotic cells + Number of late apoptotic cells)/(Number of viable cells + early apoptotic cells + late apoptotic cells + necrotic cells) x100%.

*EdU detection*. HaCaT cells were divided into the following groups: i) Blank control group; ii) 50% $IC_{50}$ capecitabine group; iii) $IC_{50}$ capecitabine group and iv) metabolite group (including acyclovir and lamivudine). Cells were uniformly seeded into 6-well plates using 2 ml of cell suspension per well and cultured at 37˚C with 5% $CO_2$ for 48 h. EdU (cat. no. C0081S; Beyotime Institute of Biotechnology) was diluted to 20 $\mu$M using cell culture medium at a ratio of 1:500. Each well was inoculated with the 20-$\mu$M diluted EdU solution and incubated for an additional 2 h at 37˚C. Following incubation, the medium was removed and cells were fixed with 4% paraformaldehyde (cat. no. 80096618; Sinopharm Chemical Reagent Co., Ltd.) for 15 min, followed by three washes with PBS. Cells were subsequently permeabilized with 0.5% Triton-X-100 (cat. no. ST795; Beyotime Institute of Biotechnology) for 20 min. After permeabilization, cells were stained with EdU staining solution (cat. no. C0078S; Beyotime Institute of Biotechnology) in the dark for 30 min at room temperature. Following staining, the slides were washed three times with PBS, and cell nuclei were stained with DAPI (cat. no. D9542; Sigma-Aldrich; Marck KGaA) for 5 min in the dark at room temperature. After washing with PBS, the cells were mounted with an anti-fluorescence quenching agent (cat. no. 0100-01; Southern Biotech) at room temperature and visualized using a fluorescence microscope (Nikon ECLIPSE Ts2; Nikon Corporation). The imaging system used was a Nikon DS-Fi3 (Nikon Corporation).

*Calcein-AM/PI staining*. HaCaT cells were divided into the following groups: i) Blank control group; ii) 50% $IC_{50}$ capecitabine group; iii) $IC_{50}$ capecitabine group and iv) metabolite group (including acyclovir and lamivudine). In total, 1 ml of cell suspension was added per well in a pre-prepared 12-well plate with coverslips and cells were cultured overnight at 37˚C in a 5% $CO_2$ incubator (Thermo Fisher Scientific, Inc.). Calcein AM (1,000X) and PI (1,000X; cat. no. C2015S; Beyotime Institute of Biotechnology) were diluted in detection buffer to prepare a 1X Calcein AM/PI working solution. In total, 500 $\mu$l of the working solution was added to each well. Cells were subsequently incubated at 37˚C in the dark for 30 min. Images were captured using an inverted fluorescence microscope (ECLIPSE Ts2; Nikon Corporation).

*Statistical analyses*. GraphPad Prism version 10.1.1 (Dotmatics) was used for statistical analyses. The Student's unpaired t-tests and fold difference analysis were used to calculate P-values between two groups. For clinical characteristics of patients, the Student's unpaired t-tests and $\chi^2$ test were

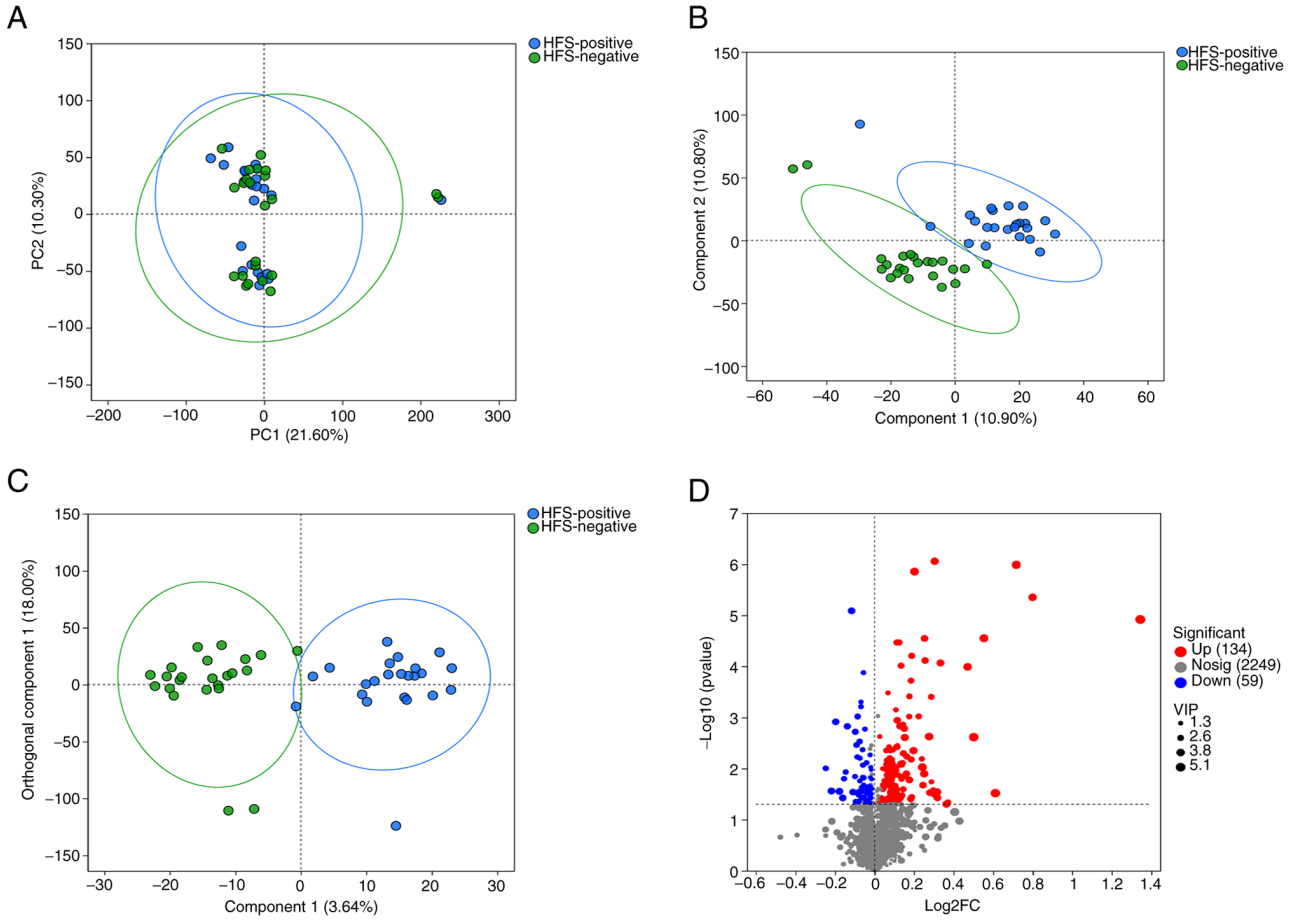


Figure 1. Multivariate statistical analyses and volcano plot of differential metabolites in HFS-positive vs. HFS-negative groups. (A) PCA score plot for HFS-positive and HFS-negative groups. (B) PLS-DA score plot between the two groups. (C) OPLS-DA score plot comparing the two groups. (D) A volcano plot was used to compare the upregulated and downregulated metabolites between HFS-positive and HFS-negative groups. PCA, principal component analysis; HFS, hand-foot syndrome; PLS-DA, least partial squares discriminant analysis; OPLS-DA, orthogonal least partial squares discriminant analysis; VIP, variable importance in the projection.

performed. P<0.05 was considered to indicate a statistically significant difference.

## Results

*Clinical characteristics of patients*. The primary characteristics of patients are summarized in Table I. In the present study, patients were categorized based on the presence of HFS. Those without symptoms were classified as the HFS-negative group, while those exhibiting symptoms were categorized as the HFS-positive group. No statistically significant differences were observed between the two groups in terms of age, sex or tumor type (P>0.05), indicating that the groups were comparable.

*Metabolomic profiles between HFS-positive and HFS-negative groups*. The raw data included QC and detection samples. In the present study, the original data was pre-processed, including filtering of missing values from the original data, simulation (missing value recoding), data normalization (normalization), QC verification and data conversion (16,17). Following pre-processing of the raw data, 1,029 positive ion metabolites and 1,413 negative ion metabolites were identified. Among them, 968 positive ion metabolites and 1,358 negative ion metabolites were present in the library. In total, 512 positive ion metabolites and 671 positive ion metabolites were annotated using KEGG. To determine the overall differences between the HFS-positive and HFS-negative groups, PCA and PLS-DA score plots were utilized. Further analysis using the OPLS-DA model identified metabolites with a VIP score of >1, a fold change (FC) of ≥1 and a P-value of <0.05 as markedly differential metabolites. A total of 193 differential metabolites were identified, with 134 upregulated and 59 downregulated in the HFS-positive group.

Results of the PCA indicated minimal within-group variability and significant between-group differences (Fig. 1A). The PLS-differential abundance (DA) score plot demonstrated a notable separation between the two groups (Fig. 1B). The OPLS-DA score plot further confirmed the distinct differences between groups, enhancing model performance (Fig. 1C). A volcano plot highlighted differential metabolites between the two groups (Fig. 1D). Acyclovir's log2FC was 0.7171, P-value=$1.03\times10^{-6}$, -log10(P-value) was 5.99, Lamivudine's log2FC was 0.4707, P-value=$1.021\times10^{-4}$, -log10(P-value) was 3.991, Genistein's log2FC was -0.1607, P-value=$3.762\times10^{-2}$, -log10(P-value) was 1.4248. Lomerizine's log2FC was -0.1159, P-value=$8.17\times10^{-6}$ and -log10(P-value) was 5.0885.

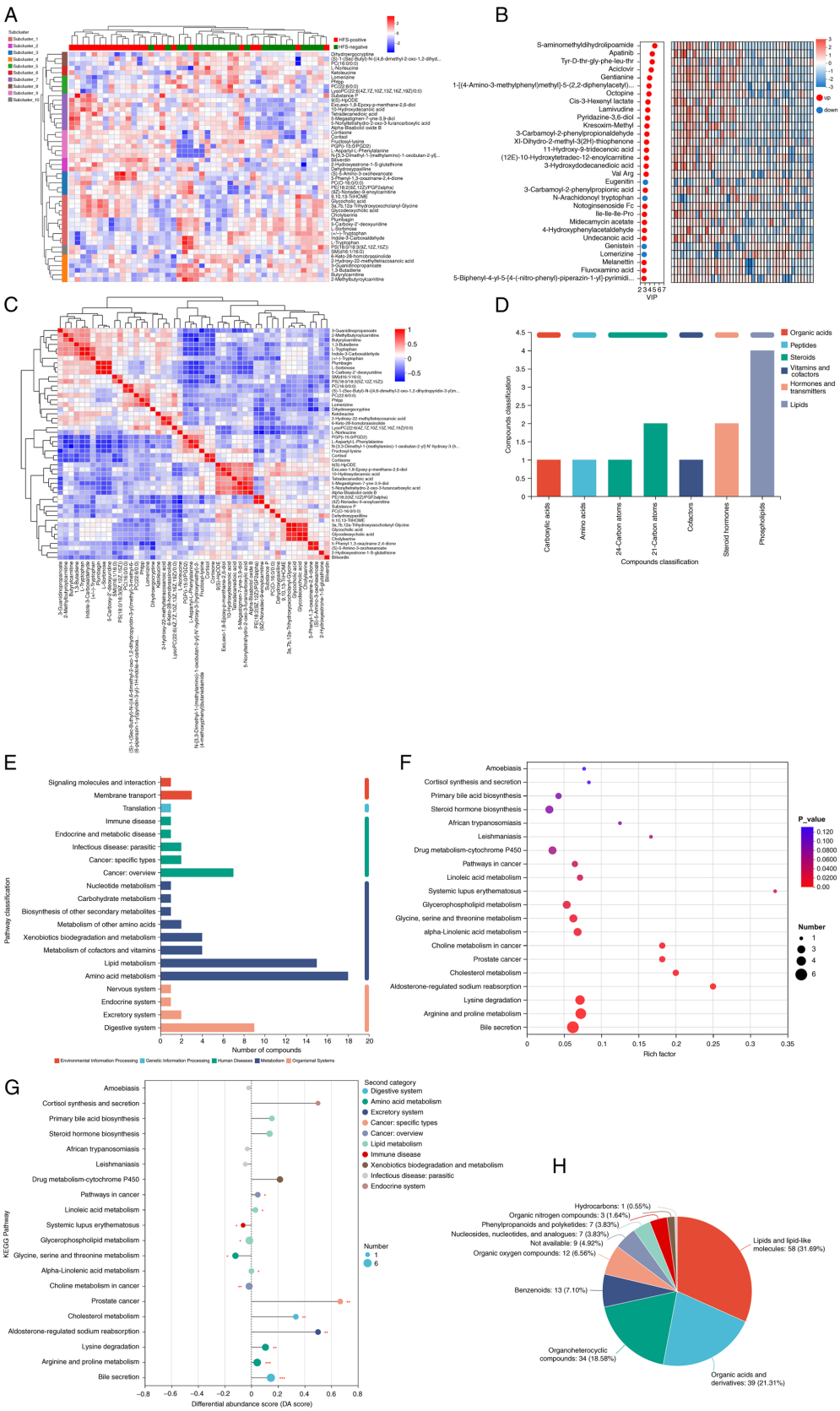


Figure 2. Comprehensive metabolomic profiling and pathway enrichment of differential metabolites in HFS-positive vs. HFS-negative groups. (A) Heatmap of significantly altered metabolites between the two groups. Red and green represent HFS-positive and HFS-negative groups, respectively. (B) VIP analysis of differential metabolites between the two groups. (C) Differential metabolite correlation analysis. Names of metabolites are in the right and bottom of the figure and metabolite clustering dendrograms are in the left and top of the figure. (D) KEGG indicated the biological functions of metabolites. (E) KEGG metabolic pathways were used to classify differential metabolites into five categories; namely, environmental information processing, genetic information processing, human diseases, metabolism and organismal systems. (F) Enriched KEGG pathways of 193 differential metabolites between the HFS-positive and HFS-negative groups. (G) DA score is indicative of changes in differential metabolites in the metabolite pathway. (H) HMDB compound classification of the differential metabolites. HFS, hand-foot syndrome; VIP, variable importance in the projection; KEGG, Kyoto Encyclopedia of Genes and Genomes; DA, differential abundance; HMDB, Human Metabolome Database.

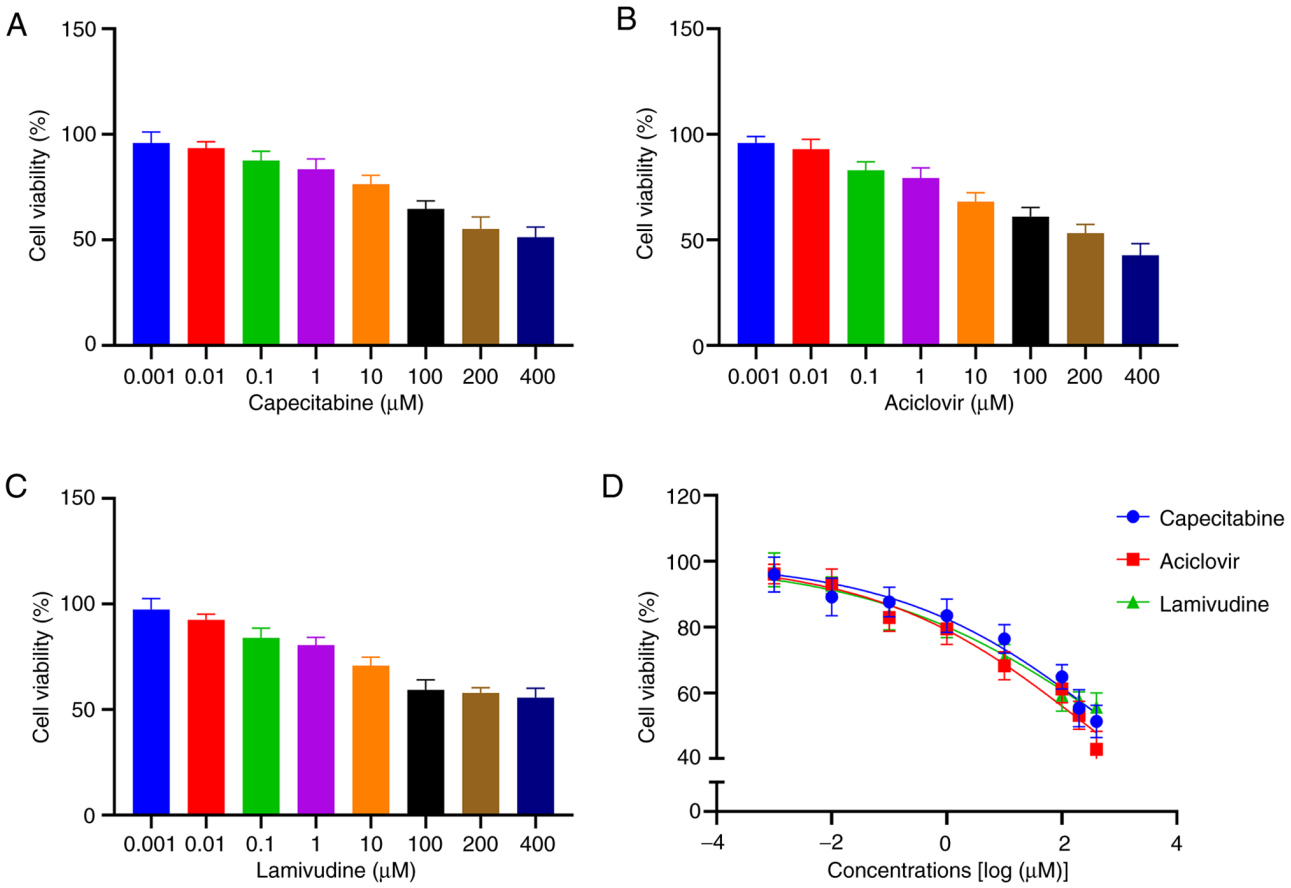


Figure 3. Dose-dependent effects of capecitabine, acyclovir and lamivudine on cell viability analyzed via non-linear regression. Cell viability (%) following treatment with (A) capecitabine, (B) acyclovir and (C) lamivudine. (D) Non-linear regression curves were used to determine the association between cell activity (%) and capecitabine, aciclovir and lamivudine concentration [Log ($\mu$M)].

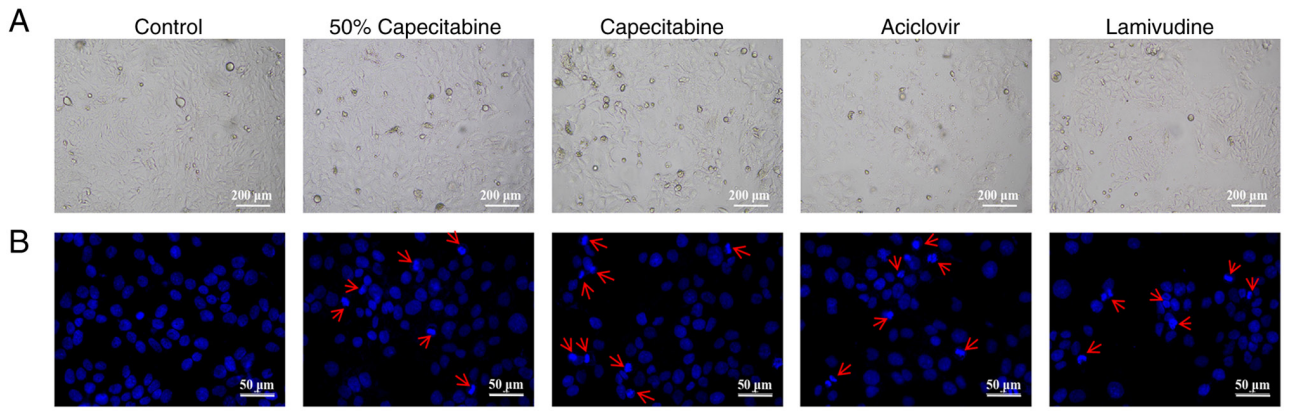


Figure 4. Effects of treatment on cell and nuclear morphology. Effects of treatment on (A) cell morphology and (B) nuclear morphology, determined using Hoechst 33258 staining. The red arrows indicate nuclear condensation following treatment.

*Differential metabolite analysis*. To further investigate the potential causes of HFS based on the differential metabolites identified between the HFS-positive and HFS-negative groups, cluster analysis was performed, including cluster and sub-cluster heatmaps (Fig. 2A). Using OPLS-DA/PLS-DA as the supervised model, different changes in predicted pairings were tested through seven-fold cross validation. VIP analysis of the first principal component identified key metabolites contributing to the classification and these were highlighted as potential biomarkers for the promotion of metabolism (Fig. 2B).

*Differential metabolite correlation analysis*. Correlation analysis aids in further understanding the mutual regulatory relationship between metabolites during biological state changes (18). The correlation coefficient is positive and negative values indicated positive and negative correlations. The closer the absolute value was to 1, the higher the positive or

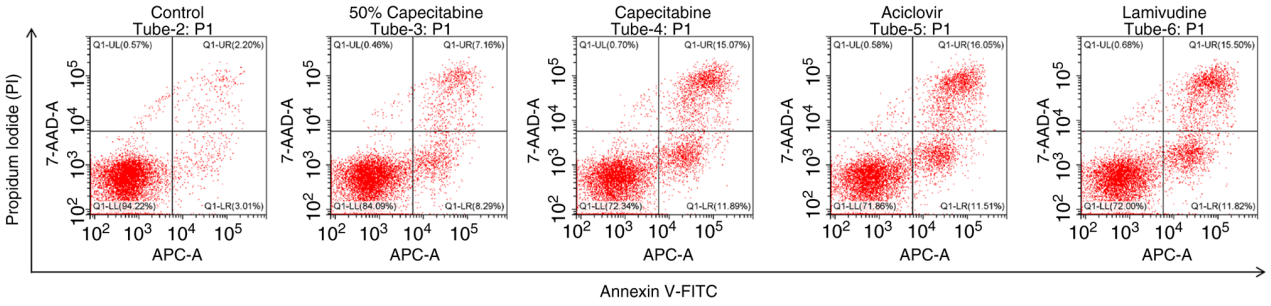


Figure 5. The apoptosis rate of cells in each group using Annexin V/PI staining. Q1-UR: Late apoptotic cells. Q1-UL: Necrotic cells. Q1-LL: Viable (negative) cells. Q1-LR: Early apoptotic cells. Total apoptosis rate (%)=(LR + UR)/(LL + LR + UR + UL) x100%. UR, upper right; LR, lower right; LL, lower left; UL, upper left.

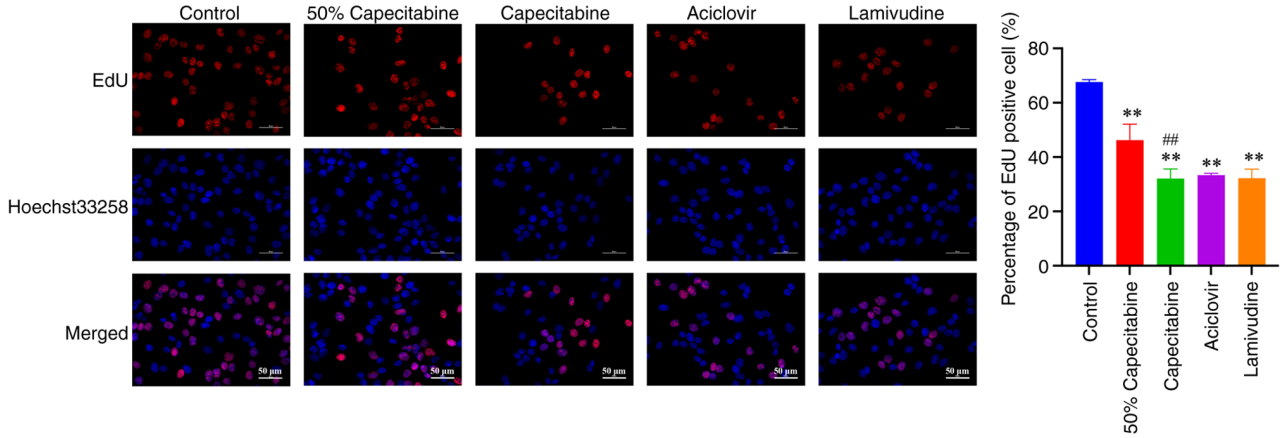


Figure 6. HaCaT cell proliferation following treatment. $^{**}$P<0.01 vs. control; $^{\#\#}$P<0.01 vs. 50% capecitabine. HaCaT, human adult keratinocyte cell line, TPA-treated cells.

negative correlation of the metabolites (Fig. 2C). Based on their biological functions, metabolites were categorized following mapping to the KEGG compound database (https://www.kegg.jp/kegg/compound/), including organic acids, peptides, steroids, vitamin and cofactors, hormones and transmitters and lipids (Fig. 2D). According to the KEGG compound identification, metabolic pathways involving the differential metabolites were identified (Fig. 2E). KEGG pathway enrichment analysis and the differential abundance score plot highlighted relevant metabolic pathways and their biological functions. Specific pathways, including bile secretion, arginine and proline metabolism, lysine degradation, glycerophospholipid metabolism, glycine, serine and threonine metabolism and alpha-linolenic acid metabolism demonstrated the highest enrichment levels (Fig. 2F). Notably, the DA score reflected the overall change of all metabolites in a metabolic pathway. A score of 1 indicated a trend towards upregulation for all differential metabolites in that pathway, while a score of -1 indicating a trend towards downregulation (Fig. 2G). The differential metabolites were classified in the HMDB as follows: Lipids and lipid-like molecules, organic acids and derivatives, organoheterocyclic compounds, benzenoids, organic oxygen compounds, nucleosides, nucleotides and analogues (Fig. 2H).

*Biological relevance of differential metabolites*. Collectively, these results suggested that the differential metabolites may be associated with various biological processes and molecular functions. Aciclovir and lamivudine are classified as organoheterocyclic compounds in HMDB and, according to the KEGG pathway analysis, these are involved in the bile secretion pathway. Previous research indicates that these compounds may exert notable neurotoxicity and immunomodulatory effects (19-22). Genistein and lomerizine, involved in KEGG metabolic pathways, demonstrated markedly alleviate various inflammatory reactions (23-25). Their presence suggested a potential role in modulating inflammatory responses associated with HFS. Lipids and lipid-like molecules and the enrichment of lipids in the differential metabolite profile highlights their potential role in cell membrane integrity and signaling pathways (26-28), which may contribute to the pathogenesis of HFS. Organic acids and derivatives, including intermediates of the TCA cycle and amino acid metabolism (29,30), may reflect alterations in energy metabolism and cellular homeostasis in response to capecitabine treatment. Thus, further *in vitro* experiments are required to verify the damaging effects of capecitabine and its metabolites on HaCaT cells and to elucidate their mechanistic roles in HFS development.

*Cytotoxicity of capecitabine and its metabolites on HaCaT cells*. HaCaT cells were treated with varying concentrations (0.001, 0.01, 0.1, 1, 10, 100, 200 and 400 $\mu$M) of capecitabine, aciclovir, genistein, lomerizine and lamivudine. Cytotoxicity was measured using the CCK-8 assay

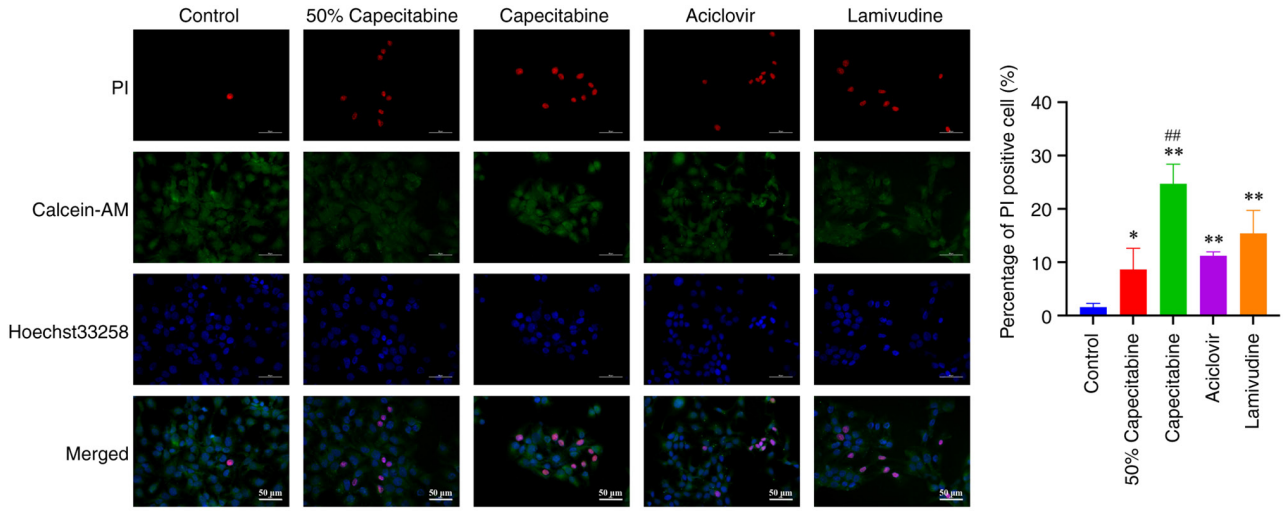


Figure 7. Calcein acetoxymethyl ester/propidium iodide double staining of HaCaT cells. $^{*}$P<0.05, $^{**}$P<0.01 vs. control; $^{\#\#}$P<0.01 vs. 50% capecitabine. HaCaT, human adult keratinocyte cell line, TPA-treated cells.

and $IC_{50}$ values were calculated. Aciclovir and lamivudine exhibited the highest levels of toxicity in HaCaT cells ($IC_{50}$ values, 278.1 and 853.5 $\mu$M, respectively) compared with genistein and lomerizine ($IC_{50}$ values, 13,982 and 1,511 $\mu$M, respectively). Notably, the $IC_{50}$ value for capecitabine was 752.2 $\mu$M. Fig. 3 illustrates the association between cell viability and concentration of aciclovir, lamivudine and capecitabine.

*Effect of capecitabine and its metabolites on cell morphology.* Based on the calculated $IC_{50}$ values, HaCaT cells were treated with 50% $IC_{50}$ capecitabine, $IC_{50}$ capecitabine, $IC_{50}$ aciclovir and $IC_{50}$ lamivudine. Microscopic observation of cell morphology (Fig. 4A) revealed a reduction in cell number and signs of apoptosis in all groups. Hoechst 33258 staining (Fig. 4B) further confirmed nuclear condensation following treatment (indicated by red arrows). Annexin V/PI staining (Fig. 5) revealed the apoptosis rate of cells in each group.

*Effects of capecitabine and its metabolites on HaCaT cell proliferation.* The EdU assay was used to determine HaCaT cell proliferation in blank control, 50% IC50 capecitabine, $IC_{50}$ capecitabine, $IC_{50}$ aciclovir and $IC_{50}$ lamivudine groups. As shown in Fig. 6, the number of EdU-positive cells in the capecitabine, aciclovir and lamivudine groups were markedly reduced and this was indicative of inhibited HaCaT cell proliferation.

*Cell viability.* Using Calcein-AM/PI dual staining, the viability of HaCaT cells was compared between control, 50% IC50 capecitabine, $IC_{50}$ capecitabine, $IC_{50}$ aciclovir and $IC_{50}$ lamivudine groups. Green fluorescence resulting from Calcein staining is indicative of live cells, while dead cells are marked using red fluorescence resulting from PI staining. As shown in Fig. 7, capecitabine, aciclovir and lamivudine groups demonstrated different rates of apoptosis, with capecitabine markedly promoting apoptosis, compared with its metabolites.

## Discussion

In the present study, 85 patients undergoing capecitabine treatment for cancer were recruited. In total, >50% of the participants developed HFS, highlighting the high incidence of capecitabine-induced HFS. This condition markedly affects a patient's quality of life. Thus, further investigations into the metabolic mechanisms underlying capecitabine and early intervention are required, without reducing therapeutic effectiveness.

The present study performed a non-targeted metabolomic analysis of blood samples, which included lipids as part of the broader metabolome. The present study did not specifically isolate or focus on lipid fractions, as this would require a targeted lipidomics approach. Instead, the goal was to capture a wide range of metabolites.

The present study analyzed plasma rather than whole blood to reduce complexity and ensure metabolite stability, as whole blood contains cellular components that can introduce variability. This approach aligns with standard practices in non-targeted metabolomics and allows for broader metabolome exploration.

The present study aimed to determine novel metabolites of capecitabine in patients with capecitabine-induced HFS. Significant differences in metabolites between HFS-positive and HFS-negative patients were observed using untargeted metabolomics. A total of 193 differential metabolites were identified, with 134 upregulated and 59 downregulated. Results of the bioinformatics analysis demonstrated that aciclovir, lamivudine, genistein and lomerizine exhibited high VIP values. Further *in vitro* validation of these compounds was performed based on the specific functions.

Results of the present study revealed that ciclovir and lamivudine exerted the highest levels of cell damage. Hochest33258 staining revealed that treatment with capecitabine, aciclovir and lamivudine led to high levels of cell damage, apoptosis and nuclear condensation. Annexin V/PI staining revealed that treatment with capecitabine, aciclovir and lamivudine led

to high rates of apoptosis. Moreover, results of EdU assays demonstrated that capecitabine, aciclovir and lamivudine inhibited HaCaT cell proliferation. Calcein-AM/PI double staining indicated cell necrosis following treatment with capecitabine, acyclovir and lamivudine, with aciclovir and lamivudine treatment inducing notably higher rates of apoptosis. *In vitro* experiments confirmed the cytotoxic effects of aciclovir and lamivudine on HaCaT cells. Collectively, these results suggested that aciclovir and lamivudine may play a role in the development of HFS.

Aciclovir is a nucleoside analog that is structurally similar to guanosine and this metabolite may cause neurotoxicity. Results of previous studies demonstrated that aciclovir-induced neurotoxicity may cause confusion, psychiatric symptoms and in some cases, seizures, myoclonus and dysarthria (22,31,32). The observed neurotoxicity is often reversible and results of previous studies suggested that it may be associated with the accumulation of aciclovir and its metabolite, 9-(carboxymethoxymethyl)guanine. Pharmacokinetic data also indicates that hepatic and renal clearance rates are closely associated with its toxicity (33,34).

Lamivudine, a nucleoside reverse transcriptase inhibitor (NRTI), is primarily associated with peripheral neuropathy, including distal sensory peripheral neuropathy (35,36) Oxygen-dependent tissues, such as the heart muscle, skeletal and smooth muscles, as well as the central and peripheral nervous systems, are susceptible to NRTI-related toxicity. NRTIs contain an azido group, which competes with natural thymidine triphosphate as a substrate for DNA polymerase γ, leading to the termination of mitochondrial DNA (mtDNA) synthesis. This inhibits both nuclear and mtDNA polymerases, causing DNA chain termination at the nucleoside analog insertion point (37). Prolonged exposure to nucleoside analogs may result in short-term mitochondrial damage. Previous studies suggested that NRTI-induced peripheral neuropathy may be caused by mitochondrial toxicity (38,39).

HFS is one of the most severe side effects associated with capecitabine treatment in patients with cancer. The observed levels of neurotoxicity are associated with the severity of HFS, with higher levels of neurotoxicity corresponding to more severe HFS. Notably, investigations that are focused on HFS risk factors have not specifically focused on grade 2 and 3 HFS (40-42). At present, research is focused on the inflammatory response in patients with HFS (43,44). Although the active component of capecitabine is 5-fluorouracil (5-FU), metabolic analysis has not yet detected this metabolite. Moreover, patients receiving systemic 5-FU alone experience fewer symptoms associated with HFS, compared with those treated with capecitabine (45). Results of *in vitro* studies demonstrate that capecitabine may induce keratinocyte death through the activation of apoptotic pathways and the reduction of mitochondrial membrane potential (46). Notably, reactive metabolites produced during metabolism may lead to drug toxicity (47,48). Therefore, further investigations are required to determine the specific role of metabolites associated with capecitabine and to further clarify the mechanisms underlying HFS. This may aid in treatment optimization, leading to personalized capecitabine therapy.

Results of the present study provided valuable insights into the cytotoxic effects of capecitabine and its metabolites, with aciclovir and lamivudine affecting cellular damage at the highest level. The identified metabolites may exhibit potential as biomarkers to predict susceptibility to HFS, enabling early identification of at-risk patients. Further investigations are required to determine the specific mechanism by which metabolites cause cell damage, leading to the development of novel treatment options. For example, inhibitors that target these specific pathways may aid in reducing the toxic effects of capecitabine on skin cells. Patients exhibiting high levels of these metabolites may benefit from personalized capecitabine dosing strategies to minimize the risk of developing HFS while maintaining therapeutic efficacy.

In conclusion, the present study used untargeted metabolomics to identify metabolites associated with capecitabine-induced HFS, offering novel insights into the metabolic pathways involved in HFS. However, the present study showed limitations, including a small sample size. Additional large-scale investigations are required to determine the specific mechanisms of capecitabine and the presence of metabolites in urine or plasma samples. Further investigations should aim to identify biomarkers for the development of personalized treatment options for HFS.

**Acknowledgments**

Not applicable.

**Funding**

The present study was supported by Nanjing Health Science and Technology Development Special Fund Project (grant no. YKK21232).

**Availability of data and materials**

The data generated in the present study may be found in the OMIX, China National Center for Bioinformation/Beijing Institute of Genomics, Chinese Academy of Sciences at the following URL https://ngdc.cncb.ac.cn/omix/release/OMIX009348.

**Authors' contributions**

YB performed all experiments, with the assistance of HC, BS, ZW, YD, YH and YW. CZ and ZS interpreted the results. YB and HC wrote the manuscript, contributed to the design of the study and collected the data. LG was involved in the conception and design of the study, provided critical interpretation of the data, and contributed substantially to revising the manuscript for important intellectual content. YB, HC and LG confirm the authenticity of all the raw data. All authors read and approved the final manuscript.

**Ethics approval and consent to participate**

The present study was conducted according to the guidelines of the Declaration of Helsinki and approved by the Institutional Ethics Committee of Nanjing Jiangning Hospital of Traditional Chinese Medicine (approval no. JZL-2021-08K-01).Written informed consent was

obtained from all individual participants included in the present study.

### Patient consent for publication

Not applicable.

### Competing interests

The authors declare that they have no competing interests.

### References


1. Jo JH, Kim YT, Choi HS, Kim HG, Lee HS, Choi YW, Kim DU, Lee KH, Kim EJ, Han JH, *et al*: Efficacy of GV1001 with gemcitabine/capecitabine in previously untreated patients with advanced pancreatic ductal adenocarcinoma having high serum eotaxin levels (KG4/2015): An open-label, randomised, Phase 3 trial. Br J Cancer 130: 43-52, 2024.
2. Primrose JN, Fox RP, Palmer DH, Malik HZ, Prasad R, Mirza D, Anthony A, Corrie P, Falk S, Finch-Jones M, *et al*: Capecitabine compared with observation in resected biliary tract cancer (BILCAP): A randomised, controlled, multicentre, phase 3 study. Lancet Oncol 20: 663-673, 2019.
3. Knikman JE, Rosing H, Guchelaar HJ, Cats A and Beijnen JH: A review of the bioanalytical methods for the quantitative determination of capecitabine and its metabolites in biological matrices. Biomed Chromatogr 34: e4732, 2020.
4. Alzahrani SM, Al Doghaither HA, Al-Ghafari AB and Pushparaj PN: 5-Fluorouracil and capecitabine therapies for the treatment of colorectal cancer (Review). Oncol Rep 50: 175, 2023.
5. Wang Z, Li X, Yang Y, Zhang F, Li M, Chen W, Gao S and Chen W: A sensitive and efficient method for determination of capecitabine and its five metabolites in human plasma based on one-step liquid-liquid extraction. J Anal Methods Chem 2019: 9371790, 2019.
6. King TL, Voon PJ, Yuen KH and Mohamed Noor DA: Hand-foot syndrome in cancer patients on capecitabine: Examining prevalence, impacts, and associated risk factors at a cancer centre in Malaysia. Support Care Cancer 32: 345, 2024.
7. de Queiroz MVR, de Medeiros ACTR, Toledo SP, de Abreu Sarmenghi KD and de Vasconcellos VF: Hand-foot syndrome caused by capecitabine: incidence, risk factors and the role of dermatological evaluation. Ecancermedicalscience 16: 1390, 2022.
8. Ahn HR, Lee SK, Youn HJ, Yun SK and Lee IJ: Stevens-Johnson syndrome and concurrent hand foot syndrome during treatment with capecitabine: A case report. World J Clin Cases 9: 4279-4284, 2021.
9. Lou Y, Wang Q, Zheng J, Hu H, Liu L, Hong D and Zeng S: Possible pathways of capecitabine-induced hand-foot syndrome. Chem Res Toxicol 29: 1591-1601, 2016.
10. Hiromoto S, Kawashiri T, Yamanaka N, Kobayashi D, Mine K, Inoue M, Uchida M and Shimazoe T: Use of omeprazole, the proton pump inhibitor, as a potential therapy for the capecitabine-induced hand-foot syndrome. Sci Rep 11: 8964, 2021.
11. Lu W, Huang Z, Chen S, Lv H, Chen X, Lei J, Ke C, Hong C, Wei Y, Su R, *et al*: The effectiveness of EVOSKIN(R)Palm and sole moisturizing cream in treating capecitabine-associated hand-foot syndrome: A randomized double-blind clinical trial. Ann Palliat Med 10: 3009-3017, 2021.
12. Schag CC, Heinrich RL and Ganz PA: Karnofsky performance status revisited: Reliability, validity, and guidelines. J Clin Oncol 2: 187-193, 1984.
13. Freites-Martinez A, Santana N, Arias-Santiago S and Viera A: Using the common terminology criteria for adverse events (CTCAE-Version 5.0) to evaluate the severity of adverse events of anticancer therapies. Actas Dermosifiliogr (Engl Ed) 112: 90-92, 2021 (In English, Spanish).
14. R Core Team: R: A language and environment for statistical computing. R Foundation for Statistical Computing, Vienna, 2021.
15. Li C, Zhang J, Wu R, Liu Y, Hu X, Yan Y and Ling X: A novel strategy for rapidly and accurately screening biomarkers based on ultraperformance liquid chromatography-mass spectrometry metabolomics data. Anal Chim Acta 1063: 47-56, 2019.
16. Karaman I: Preprocessing and pretreatment of metabolomics data for statistical analysis. Adv Exp Med Biol 965: 145-161, 2017.
17. Yang J, Zhao X, Lu X, Lin X and Xu G: A data preprocessing strategy for metabolomics to reduce the mask effect in data analysis. Front Mol Biosci 2: 4, 2015.
18. Liang JH, Lin Y, Ouyang T, Tang W, Huang Y, Ye W, Zhao JY, Wang ZN and Ma CC: Nuclear magnetic resonance-based metabolomics and metabolic pathway networks from patient-matched esophageal carcinoma, adjacent noncancerous tissues and urine. World J Gastroenterol 25: 3218-3230, 2019.
19. Berry L and Venkatesan P: Aciclovir-induced neurotoxicity: Utility of CSF and serum CMMG levels in diagnosis. J Clin Virol 61: 608-610, 2014.
20. Perez Valero I, Cabello A, Ryan P, De La Fuente-Moral S, Santos I, Vivancos MJ, Gonzalez A, Gorgolas M, Cuevas G, Diaz De Santiago A, *et al*: Randomized trial evaluating the neurotoxicity of dolutegravir/abacavir/lamivudine and its reversibility after switching to elvitegravir/cobicistat/emtricitabine/tenofovir alafenamide: GESIDA 9016. Open Forum Infect Dis 7: ofaa482, 2020.
21. Tarpey AE, Loranger A, Plambeck R and Malesker MA: Neurotoxicity secondary to valacyclovir. J Pharm Technol 38: 251-252, 2022.
22. Vonberg FW, Dawson A, Scott G and Davies N: Aciclovir-induced neurotoxicity. Pract Neurol 23: 157-159, 2023.
23. Garbiec E, Cielecka-Piontek J, Kowalowka M, Holubiec M and Zalewski P: Genistein-opportunities related to an interesting molecule of natural origin. Molecules 27: 815, 2022.
24. Park JH, Hwang JW, Lee HJ, Jang GM, Jeong YJ, Cho J, Seo J and Hoe HS: Lomerizine inhibits LPS-mediated neuroinflammation and tau hyperphosphorylation by modulating NLRP3, DYRK1A, and GSK3α/β. Front Immunol 14: 1150940, 2023.
25. Wei TT, Chandy M, Nishiga M, Zhang A, Kumar KK, Thomas D, Manhas A, Rhee S, Justesen JM, Chen IY, *et al*: Cannabinoid receptor 1 antagonist genistein attenuates marijuana-induced vascular inflammation. Cell 185: 2387-2389. e23, 2022.
26. Hannun YA and Obeid LM: Principles of bioactive lipid signalling: Lessons from sphingolipids. Nat Rev Mol Cell Biol 9: 139-150, 2008.
27. van Meer G, Voelker DR and Feigenson GW: Membrane lipids: Where they are and how they behave. Nat Rev Mol Cell Biol 9: 112-124, 2008.
28. Dennis EA and Norris PC: Eicosanoid storm in infection and inflammation. Nat Rev Immunol 15: 511-523, 2015.
29. Brosnan JT: Interorgan amino acid transport and its regulation. J Nutr 133 (6 Suppl 1): 2068S-2072S, 2003.
30. DeBerardinis RJ and Chandel NS: Fundamentals of cancer metabolism. Sci Adv 2: e1600200, 2016.
31. Arlemalm A, Hellden A, Karlsson L and Carlsson B: Rapid determination of acyclovir, its main metabolite 9-carboxymethoxymethylguanine, ganciclovir, and penciclovir in human serum using LC-MS/MS. Biomed Chromatogr 36: e5315, 2022.
32. Abuhelwa Z, Beran A, Venkataramany BS, Hinch BT and Assaly R: Concurrent nephrotoxicity and neurotoxicity induced by oral valacyclovir in a patient with previously normal kidney function. Cureus 14: e23693, 2022.
33. Aboelezz A and Mahmoud SH: Acyclovir dosing in herpes encephalitis: A scoping review. J Am Pharm Assoc (2003) 64: 102040, 2024.
34. Takeda S, Ueno S, Zenda R, Muto K, Iseki K and Harada K: Simultaneous analysis of acyclovir and its metabolite using hydrophilic interaction liquid chromatography-tandem mass spectrometry. J Anal Toxicol 48: 204-209, 2024.
35. Leger PD, Johnson DH, Robbins GK, Shafer RW, Clifford DB, Li J, McLaren PJ and Haas DW: Genome-wide association study of peripheral neuropathy with D-drug-containing regimens in AIDS clinical trials Group protocol 384. J Neurovirol 20: 304-308, 2014.
36. Bokore A, Korme B and Bayisa G: Determinants of anti-retroviral regimen changes among HIV/AIDS patients of east and west Wollega zone health institutions, Oromia region, west Ethiopia: A cross-sectional study. BMC Pharmacol Toxicol 19: 28, 2018.
37. Dalakas MC: Peripheral neuropathy and antiretroviral drugs. J Peripher Nerv Syst 6: 14-20, 2001.

38. Youle M: Acetyl-L-carnitine in HIV-associated antiretroviral toxic neuropathy. CNS Drugs 21 (Suppl 1): 25-30; discussion 45-26, 2007.
39. Dagan T, Sable C, Bray J and Gerschenson M: Mitochondrial dysfunction and antiretroviral nucleoside analog toxicities: What is the evidence? Mitochondrion 1: 397-412, 2002.
40. Chantharakhit C and Sujaritvanichpong N: Predictive factors for the development of capecitabine-induced hand-foot syndrome: A retrospective observational cohort study. Ann Med Surg (Lond) 86: 73-77, 2024.
41. Yap YS, Kwok LL, Syn N, Chay WY, Chia JWK, Tham CK, Wong NS, Lo SK, Dent RA, Tan S, *et al*: Predictors of hand-foot syndrome and pyridoxine for prevention of capecitabine-induced hand-foot syndrome: A Randomized clinical trial. JAMA Oncol 3: 1538-1545, 2017.
42. Kwakman JJM, Simkens LHJ, van Rooijen JM, van de Wouw AJ, Ten Tije AJ, Creemers GJM, Hendriks MP, Los M, van Alphen RJ, Polee MB, *et al*: Randomized phase III trial of S-1 versus capecitabine in the first-line treatment of metastatic colorectal cancer: SALTO study by the Dutch colorectal cancer group. Ann Oncol 28: 1288-1293, 2017.
43. Santhosh A, Sharma A, Bakhshi S, Kumar A, Sharma V, Malik PS, Pramanik R, Gogia A, Prasad CP, Sehgal T, *et al*: Topical diclofenac for prevention of capecitabine-associated hand-foot syndrome: A double-blind randomized controlled trial. J Clin Oncol 42: 1821-1829, 2024.
44. Lian S, Zhang X, Zhang Y and Zhao Q: Pyridoxine for prevention of hand-foot syndrome caused by chemotherapy agents: A meta-analysis. Clin Exp Dermatol 46: 629-635, 2021.
45. Azuma Y, Hata K, Sai K, Udagawa R, Hirakawa A, Tohkin M, Ryushima Y, Makino Y, Yokote N, Morikawa N, *et al*: Significant association between hand-foot syndrome and efficacy of capecitabine in patients with metastatic breast cancer. Biol Pharm Bull 35: 717-724, 2012.
46. Chen M, Chen J, Peng X, Xu Z, Shao J, Zhu Y, Li G, Zhu H, Yang B, Luo P and He Q: The contribution of keratinocytes in capecitabine-stimulated hand-foot-syndrome. Environ Toxicol Pharmacol 49: 81-88, 2017.
47. Guengerich FP and MacDonald JS: Applying mechanisms of chemical toxicity to predict drug safety. Chem Res Toxicol 20: 344-369, 2007.
48. Park SY, Kim MW, Kang JH, Hwang JH, Choi H, Park J, Seong JK, Yoon YS and Oh SH: Loss of Ninjurin1 alleviates acetaminophen-induced liver injury via enhancing AMPKα-NRF2 pathway. Life Sci 350: 122782, 2024.

Copyright © 2025 Bai et al. This work is licensed under a Creative Commons Attribution-NonCommercial-NoDerivatives 4.0 International (CC BY-NC-ND 4.0) License.